PNAS RESEARCH ARTICLE | CELL BIOLOGY OPEN ACCESS

The interplay of environmental luminance and genetics in the retinal dystrophy induced by the dominant RPE65 mutation

Wenjing Wu[a], Yusuke Takahashi[a,b], Henry Younghwa Shin[a], Xiang Ma[a], Gennadiy Moiseyev[a,1], and Jian-Xing Ma[a,b,1]

Edited by Vladimir Kefalov, University of California, Irvine, CA; received August 17, 2021; accepted January 11, 2022 by Editorial Board Member Jeremy Nathans

The retinol isomerase retinal pigment epithelium (RPE) 65 is a key enzyme in the visual cycle that regenerates the chromophore, 11-*cis*-retinal, required for vision in all vertebrates. Mutations in *RPE65* are associated with blinding diseases. D477G (C.1430G > A) is the only known *RPE65* variant to cause autosomal dominant retinitis pigmentosa. Previously, we reported that heterozygous *D477G* knockin (KI) mice maintained in dim-light conditions exhibited delayed visual chromophore regeneration and slowed recovery of photoreceptor sensitivity following visual pigment photobleaching. However, heterozygous *D477G* KI mice did not manifest detectable decline in full-field electroretinography (ERG) or in abnormal retinal structure, relative to the WT mice. In the present study, when maintained under the physiological relevant light intensity (2,000 lx), the heterozygous *D477G* KI mice displayed degenerative retina features, including reduced scotopic ERG amplitudes and thinning of the retinal layers, recapitulating that observed in human patients. In the same retinas, we also detected increased free opsin levels and up-regulated GFAP expression. Molecularly, we found reduced RPE65 and LRAT (lecithin: retinol acyltransferase) levels, decreased retinol isomerase activity, and altered subcellular localization and membrane association of RPE65 in the RPE of heterozygous *D477G* KI mice. Moreover, the D477G mutant, both in vivo and in vitro, formed protein complexes with WT-RPE65, leading to a reduction in RPE65 protein stability, which could not be completely rescued by the addition of MG132, a proteasome inhibitor of ubiquitin-dependent protein degradation. Altogether, our findings uncovered the dominant-negative nature of the D477G mutation and highlighted the importance of the light environment in the mechanism of its pathogenicity.

retinal degeneration | photoreceptor | RPE65 | visual cycle

Significance

In humans, genetic mutations in the retinal pigment epithelium (RPE) 65 are associated with blinding diseases, for which there is no effective therapy alleviating progressive retinal degeneration in affected patients. Our findings uncovered that the increased free opsin caused by enhancing the ambient light intensity increased retinal activation, and when compounded with the RPE visual cycle dysfunction caused by the heterozygous D477G mutation and aggregation, led to the onset of retinal degeneration.

Hereditary retinal diseases are a major cause of childhood blindness, affecting 1 in 1,000 people worldwide (1, 2). Mutations in over 300 genes expressed in both the photoreceptor (PR) and the retinal pigment epithelium (RPE) cause irreparable blindness in humans (RetNet). In the United States, mutations in the *RPE65* gene encoding the RPE specific retinol isomerase RPE65 account for no less than 13% of all inherited retinal degenerations (3, 4). These mutations cause Leber congenital amaurosis, early onset severe retinal dystrophy, and retinitis pigmentosa (RP) (5, 6). Collectively, these disorders manifest progressive vision loss, though differing in age of onset and degrees of severity, eventually leading to the loss of functional vision (7). As the cause of these ocular diseases is aberrant genetics, the contribution of environmental factors in the progression of these dystrophies remains to be elucidated.

The active light-sensing unit in vertebrate PR consists of the opsin protein and chromophore: 11-*cis*-retinal (11-*cis*-RAL), a vitamin A derivative. Photo-isomerization of the chromophore to all-*trans*-retinal (all-*trans*-RAL) triggers opsin activation, initiating phototransduction. All-*trans*-RAL is transported from the PRs to the RPE to regenerate 11-*cis*-RAL via a series of enzymatic reactions collectively termed the visual cycle. RPE65 is the only isomerase that catalyzes the final conversion of all-*trans*-retinyl ester to 11-*cis*-retinol (11-*cis*-ROL) and is indispensable to the vision process (8–10).

As of this writing, over 100 pathogenic mutations spanning all 14 exons of the *RPE65* gene have been identified in the human population. Almost all of these mutations are recessively inherited and affect its isomerase function. While screening for causative genes that lead to choroideremia, Bowne et al. (5), in patients of Irish heritage, uncovered the first pathogenic dominant-acting mutation of RPE65. A single-nucleotide substitution at exon 13 of the *RPE65* gene; a c.1430A > G caused a missense mutation, an aspartic acid to glycine (D477G). Following the first discovery of the *D477G* mutation, the same mutation was identified in a subpopulation of patients with autosomal dominant RP (adRP) of unknown etiology (11).

Author affiliations: [a]Department of Physiology, University of Oklahoma Health Sciences Center, Oklahoma City, OK 73104; and [b]Harold Hamm Diabetes Center, University of Oklahoma Health Sciences Center, Oklahoma City, OK 73104

Author contributions: W.W., Y.T., G.M., and J.-X.M. designed research; W.W., Y.T., H.Y.S., X.M., and G.M. performed research; H.Y.S. contributed new reagents/analytic tools; W.W., H.Y.S., X.M., and G.M. analyzed data; and W.W., G.M., and J.-X.M. wrote the paper.

The authors declare no competing interest.

This article is a PNAS Direct Submission. V.K. is a guest editor invited by the Editorial Board.

Copyright © 2022 the Author(s). Published by PNAS. This open access article is distributed under Creative Commons Attribution-NonCommercial-NoDerivatives License 4.0 (CC BY-NC-ND).

[1]To whom correspondence may be addressed. Email: Gennadiy-Moiseyev@ouhsc.edu or Jian-xing-ma@ouhsc.edu.

This article contains supporting information online at http://www.pnas.org/lookup/suppl/doi:10.1073/pnas.2115202119/-/DCSupplemental.

Published March 10, 2022.

Although typical RP patients develop vision loss from the peripheral visual fields due to rod PR dysfunction, individuals affected by heterozygous *RPE65-D477G* mutation exhibit various retinal degeneration phenotypes, including the simultaneous loss of both peripheral and central vision, that may involve choroidal atrophy and often include macula and RPE perturbations (12). The onset of visual impairment among the *D477G* patients occurs at various ages, and the degree of retinal degeneration can be independent of the extent of the decline in visual function (5, 13).

Four groups have generated five *D477G* knockin (KI) mouse models to study the pathophysiology of the mutant in vivo (11, 14). Similar to the heterogeneous clinical features of the D477G adRP patients, the reported impacts of the mutation were diverse. Our group reported a delayed chromophore regeneration after photobleaching, but otherwise normal in retina morphology and function in the heterozygote *D477G* KI (*WT/KI*) mice (15). Choi et al. (16) found that both the heterozygote and the homozygote *D477G* KI (*KI/KI*) mice displayed minimal age-dependent changes in retinal morphology and function. Structure model analysis of a chimeric apocarotenoid-15,15′-oxygenase protein with the *D477G* mutation in a loop structure predicted abnormal protein–protein interactions (16). In 2019, Li et al. (17) generated *D477G* KI model with the CRISPR/Cas9 technology and identified a splicing defect in variant mRNA manifesting as reduced *RPE65* levels. However, mild retinal changes were detected only in the light-stressed *KI/KI* mice. Kiang et al. (14) recently humanized their *D477G KI* mice and reported that the model revealed no apparent structural or functional phenotypes in the *WT/KI* or the *KI/KI* mice in either the Met450 or Leu450 *RPE65* background. As yet, none of the heterozygous *D477G* KI mouse models have recapitulated the visual and morphological defects found in the human patients or provided a satisfactory explanation for the observed dominant RP transmission pattern in the human *D477G* inheritance. The proposed pathogenic molecular mechanisms for retinal dysfunction and degeneration caused by the *D477G* mutation remain inconclusive.

Kenna et al. (11) recently published for the first time an improvement of visual function in three of five *D477G* patients with a 1-wk retinoid supplementation, although the retinal structure in these patients was not examined. Clinical reports for other RPE65 mutations showed that an initial recovery of visual function by either visual chromophore replenishment or expression of *RPE65* failed to alleviate retinal degeneration and vision loss progression for longer periods (18–21). The molecular basis of *D477G* pathogenesis needs to be characterized to implement effective treatments.

Here we report retinal dysfunction and morphological changes in heterozygous *D477G* KI (*WT/KI*) mice that resembled the phenotypes observed in patients. We show that environmental light exposure influenced the occurrence of retinal dysfunction in the *WT/KI* mice. The variable environmental luminance may explain the various disease severities and ages of onset observed in the patients with *D477G*-mediated adRP. We demonstrate that D477G causes atypical protein–protein interactions with WT-RPE65, leading to RPE65 protein degradation and reduced retinol isomerase activity relative to heterozygous *RPE65* knockout (KO). We addressed the dominant-negative nature of the mutation by comparing *WT/KI* to *RPE65* KO heterozygotes (*WT/KO*). It is well documented that one copy of the functional *RPE65* gene is sufficient to maintain normal retinal health and vision in both human and rodent models (22, 23). Here, we demonstrate that the appearance of retinal dysfunction was not due to haploinsufficiency, but rather due to the dominant-negative nature of D477G. This study also elucidates the relationship between environmental light and vision impairment induced by gene mutations.

Results

Heterozygous *D477G* KI (*WT/KI*) Mice Raised under Daylight Luminance Showed Exacerbated Visual Dysfunction Compared with That of the Heterozygous *RPE65* KO (*WT/KO*) Mice. Previous studies detected no visual functional differences between the heterozygous *D477G* knockout-in (*WT/KI*) and the *WT/WT* mice across different ages when raised under standard mouse husbandry lighting of approximate ∼100 lx, henceforth referred to as dim light (DimL) in this study (14, 15, 17). We evaluated whether visual function is affected in the *WT/KI* and *WT/KO* mice exposed to a higher environmental daylight luminance (DayL) of 2,000 lx starting at 3 mo of age. Electroretinography (ERG) was used to examine visual function of the *WT/KI* and *WT/KO* mice at different ages exposed to DayL and compared with their littermates exposed to the DimL luminance. Representative scotopic ERG a- and b-waves in dark-adapted mice exposed to flashes of increasing light intensities (−2.4 log to 0.6 log cd·s/m^2) are shown in Fig. 1 *A–F*. The ERG responses of the rod and cone PRs (a-wave) and their corresponding second-order neuron responses (b-wave) between the *WT/KI* and *WT/KO* mice raised under DimL were similar across all ages. However, starting at 15 mo of age, the *WT/KI* mice exposed to DayL began to display reduced scotopic ERG a- and b-wave amplitudes, which further declined at 18 mo of age compared with the *WT/KO* under the same conditions (Fig. 1 *B* and *C*). Similarly, mixed cone-rod response in the *WT/KI* mice exposed to DayL was significantly lower ($P \leq 0.01$) than the *WT/KO* mice under DayL and *WT/KI* under the same conditions (Fig. 1*H*). In contrast, the *WT/KO* mice exposed to DayL conditions showed no ERG differences from their littermates raised under DimL (Fig. 1 *B* and *C*). A photopic b-wave was used to assess cone function in light-adapted mice with a constant rod-saturating background luminance of 10 cd/m^2 (24, 25). As expected, no significant difference was detected in the cone response in mice of the indicated genotypes exposed to both luminance at all the tested ages (Fig. 1*I*), consistent with previous reports in D477G-affected patients (5, 13). Our results showed that *D477G WT/KI* mice recapitulated the rod ERG decline, a common RP phenotype (12). We observed a general age-dependent global ERG decline in all groups tested (Fig. 1*A* and *SI Appendix*, Fig. S2), as expected in aging mice (26, 27).

Both DimL- and DayL-Exposed *D477G WT/KI* Mice Showed Delayed Dark Adaptation Following Visual Pigment Photobleach. Previous studies found that *D477G WT/KI* mice, compared with the *WT/WT* and the *WT/KO* mice, displayed delayed dark adaptation in the regeneration of 11-*cis*-RAL and the slower rod PR a-wave recovery (15, 18). Here we assessed whether DayL condition delays dark adaptation and 11-*cis*-RAL regeneration. We examined the recovery of rod light sensitivity following photobleaching in the *WT/KI* and *WT/KO* mice exposed to DimL and DayL at the ages of 12 and 18 mo (Fig. 2 *A* and *B*). Dark-adapted mice of indicated genotypes were exposed to the illumination of 1,000 cd/m^2 for 2 min, followed by a light flash at 10 cd·s/m^2 to confirm the completion of photobleaching. Subsequently, the mice were allowed to dark adapt while single-flash a-wave responses at 10 cd·s/m^2 were recorded every 5 min

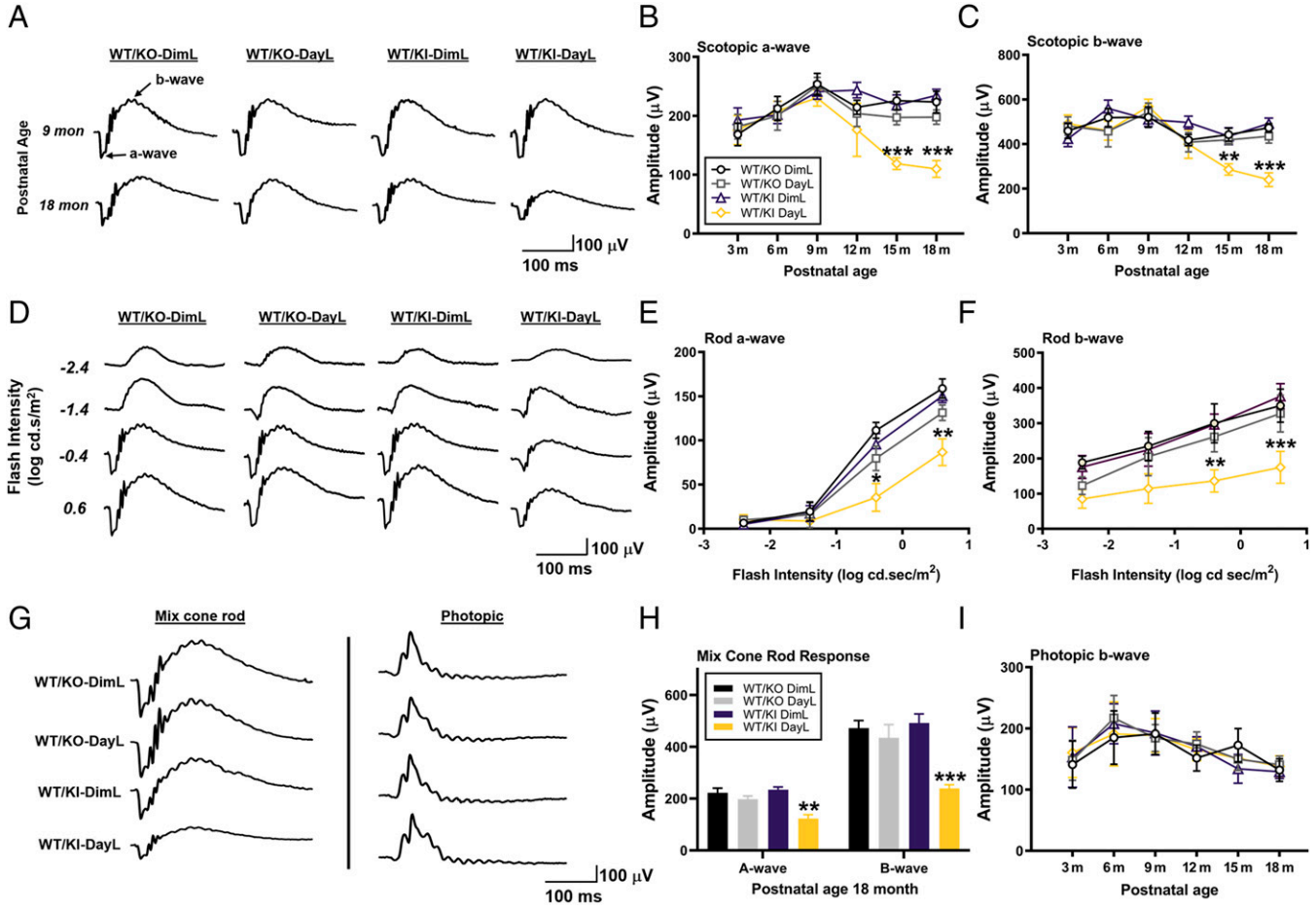

Fig. 1. ERG analysis of retina function in mice maintained under DimL and DayL luminance. (*A*) Representative dark-adapted single-flash ERG traces at 4 cd·s/m^2 in mice at 9 and 18 mo of age in the indicated genotypes. (*B* and *C*) Quantitative evaluation of scotopic response amplitudes of the *WT/KI* and *WT/KO* [a-wave (*B*), b-wave (*C*)] mice, at 3, 6, 9, 12, 15, and 18 mo of age, expose in DayL and DimL conditions. (*D*) Representative dark-adapted single-flash ERG recorded over the range of scotopic light intensities, log 0.004, 0.04, 0.4, and 4 cd·s/m^2 in 18-mo-old mice of indicated genotypes. Quantitative evaluation of a-wave (*E*) and b-wave (*F*) amplitudes in *WT/KI* and *WT/KO* mice maintained under DayL and DimL conditions; *x* axis values were log-transformed. (*G*) Representative dark-adapted single-flash ERG traces taken at 40 cd·s/m^2 (mix rod and cone) and photopic 10 cd·s/m^2 at constant background luminance of 10 cd/m^2 in mice of indicated genotypes at 18 mo of age. Quantitative evaluation of mix cone rod (*H*) and photopic (*I*) PR response in *WT/KI* and *WT/KO* mice raised in either DimL or DayL conditions. Data are presented as mean ± SEM $n = 8$ (*WT/KI* DimL & *WT/KO* DayL); $n = 10$ (*WT/KO* DimL); $n = 8$ (*WT/KI* DayL) $^*P \leq 0.05$, $^{**}P \leq 0.01$ and $^{***}P \leq 0.001$ in one-way ANOVA with Tukey's post hoc comparison.

for 1 h. At each time point, the recovered a-wave amplitude was plotted as a percentage of the initial dark-adapted rod light response. Fig. 2 *A* and *B* show the percent recovery for the mice at 12 and 18 mo. At both ages, the *WT/KI* mice exposed to both DayL and DimL conditions showed a slower rod ERG a-wave recovery rate compared with the *WT/KO* mice. In addition, at 18 mo of age, the *WT/KI* mice exposed to DayL exhibited a slower recovery rate to the initial dark-adapted ERG amplitude than littermates raised under DimL. As this difference was not manifested in the 12 mo of age group, our data suggested an age-dependent component in the progression of vision impairment by the D477G mutation. Taken together, the delayed chromophore regeneration in the heterozygous *D477G* KI mice and observations reported by Choi et al. (16) and us (15) suggest that a single copy of *D477G* mutation is sufficient to delay visual pigment regeneration even prior to the onset of retinal function decline (Fig. 2 *B* and *C*).

DayL-Exposed Heterozygous *D477G WT/KI* Mice Showed Lower Isomerase Activity than Heterozygous *WT/KO* Mice. We next investigated whether RPE65 enzymatic activity in the *D477G WT/KI* mice is affected, resulting in a delayed a-wave recovery rate. Isomerase activity assay was performed using the eye-cup homogenates from the *WT/KI* mice, and *WT/KO* mice were incubated with tritium-labeled all-*trans*-retinol. The levels of the generated 11-*cis*-ROL over 2-h incubation were measured by HPLC (Fig. 2 *D*, *Left*). The *WT/KI* mice generated significantly lower 11-*cis*-ROL levels than the *WT/KO* (Fig. 2 *D*, *Right*). This suggested that the isomerase activity in the DayL-exposed *WT/KI* RPE was attenuated, which might explain the delayed recovery of PR sensitivity.

Heterozygous *D477G* KI Mice Exposed to DayL Showed Retina Degeneration. We and others have reported that *D477G WT/KI* mice showed normal retina morphology when reared under DimL (14, 15, 17). Here we assessed the consequences of DayL exposure on the retinal structure of the *WT/KI* mice. In the *WT/KI* and *WT/KO* mice, retina integrity was evaluated by light microscopy and spectral-domain optical coherence tomography (SD-OCT) imaging. DimL-raised *WT/KI* and *WT/KO* mice showed no detectable differences in their retinal structure (Fig. 3 *A*, *a* and *c*). However, under DayL conditions, the *WT/KI* mice exhibited a decreased total retina thickness (TRT), specifically in the outer nuclear layer (ONL), relative to the *WT/KO* mice under the same condition, as shown on the H&E-stained retina cross-sections (Fig. 3 *A*, *d–f*) and by histological analysis of the

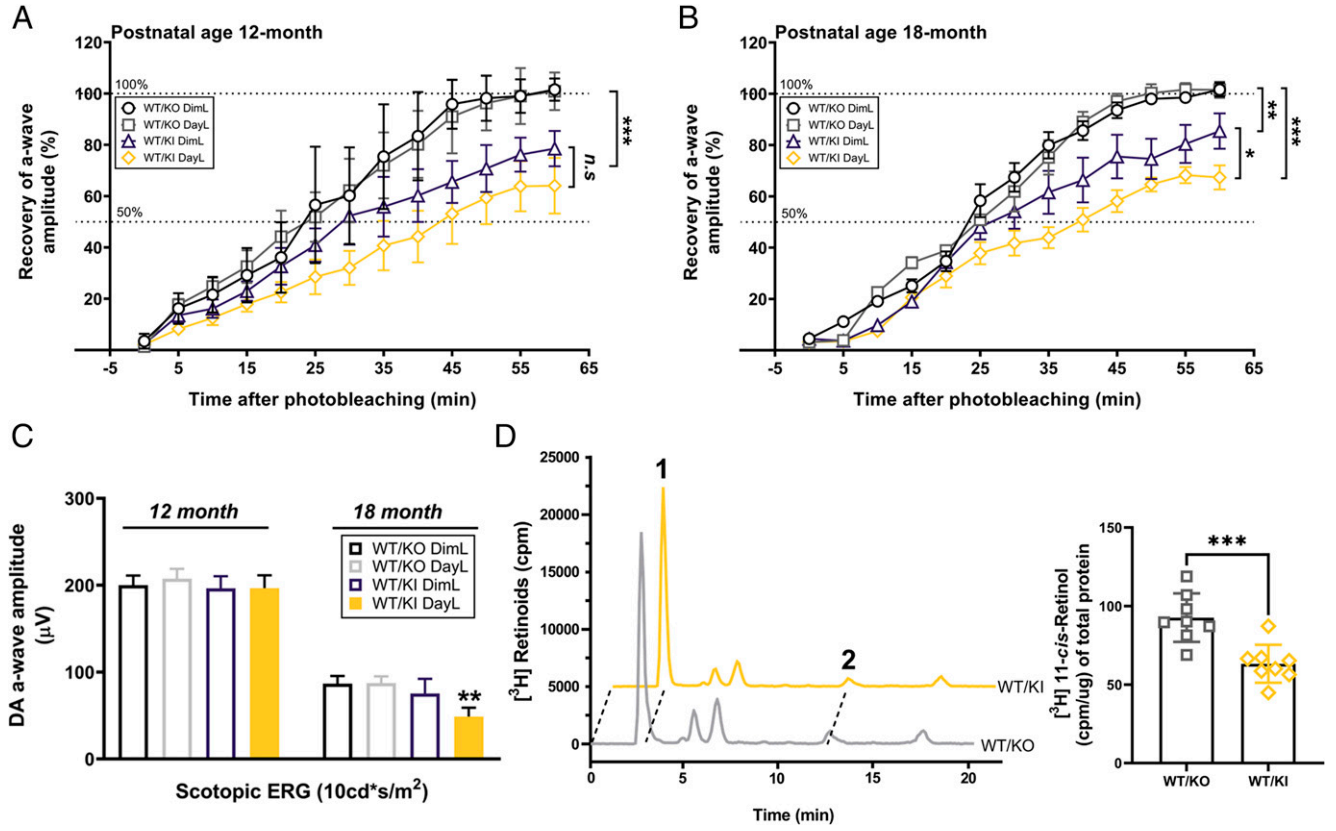

Fig. 2. Delayed rod PR a-wave recovery and reduced isomerase activity in dark-adapted heterozygous *RPE65 D477G* KI (*WT/KI*) mice. ERG a-wave recovery was evaluated after exposing dark-adapted mice maintained under DayL and DimL, to light at 1,000 cd/m^2 for 2 min. Subsequent single-flash ERG at 10 cd·s/m^2 was recorded every 5 min to evaluate the recovery of rod sensitivity in the photobleached mice of indicated genotypes. Percent (%) a-wave recovery was plotted with postbleaching amplitude taken 5 min against initial a-wave dark-adapted amplitude after visual pigment bleach in mice at the ages of 12 mo (*A*) and 18 mo (*B*). The dotted line indicates 50% and 100% recovery points on the graphs. (*C*) Prephotobleach a-wave amplitude was recorded at 10 cd·s/m^2 in dark-adapted mice. This value was taken as 100% recovery. Data are presented as mean ± SEM $n = 10$ for each group $^*P < 0.05$, $^{**}P < 0.01$, $^{***}P < 0.001$ in one-way ANOVA with Tukey's post hoc comparison. (*D*) Representative HPLC chromatograms show separation of retinoids extracted from the eye-cups of 1-y-old DayL-raised mice. Peak 1, retinyl esters; peak 2, 11-*cis*-ROL. Quantification (*Right*) of 11-*cis*-ROL in the extracts showed a significant difference between the two groups. Each point represents data from a single mouse. Data are presented as mean ± SEM $n = 8$ for each group. Statistical significance was assessed by unpaired *t* test with Tukey's post hoc comparison. $^{***}P < 0.001$.

ONL (Fig. 3*B*). Furthermore, SD-OCT image in the DayL-exposed *WT/KI* mice showed significant reductions in TRT, due to ONL, and outer segment (OS) layer thinning (Fig. 3 *D* and *E*). As expected, no retina morphological changes were detected in the *WT/KO* mice under DimL and DayL (Fig. 3 *A*, *a*–*c*). In some of the DayL-exposed *WT/KI* mice, we observed outer retinal tubulation (ORT) (Fig. 3 *A*, *e* and *D*, *e*), a type of retina anomaly seen in some of the D477G patients (5, 12, 13).

Heterozygous *D477G* KI Mice Exhibited Reduced RPE65 and LRAT Protein Levels. As previously reported, compared with the *RPE65 WT/WT*, *D477G WT/KI* and *KI/KI* showed decreased RPE65 protein levels in RPE cells (15). We compared RPE65 levels in the DimL-exposed *WT/KI* and *WT/KO* mice at postnatal day (PD) 120. At PD 120, RPE65 levels were significantly reduced in the *WT/KO* and even more in the *WT/KI* mice, compared with age-matched *WT/WT* mice (Fig. 4 *A* and *B*). Interestingly, at PD 120, levels of LRAT (lecithin: retinol acyltransferase) protein were also decreased in the *WT/KI* and *KI/KI* eye-cups, relative to *WT/WT* and *WT/KO* mice (Fig. 4*C*). Levels of other visual cycle-related proteins did not show significant changes between the genotypes at PD 120 (Fig. 4 *D*–*F*).

D477G Induced Abnormal RPE65 Protein Aggregation. We investigated whether replacing the negatively charged aspartate residue with the neutral glycine in the *D477G* mutant caused abnormal structural alterations and protein interaction. Nonreducing sucrose density sedimentation was performed on eye-cup homogenates from the indicated genotypes. Protein complexes were resolved by density on a continuous 5 to 20% sucrose gradient divided into 13 equal volume fractions (the 1st fraction the lowest/lightest molecular weight and the 13th fraction including pellet); the fractions were analyzed by immunoblotting with an anti-RPE65 antibody (Fig. 5*A*). Compared with those in the *WT/WT* and *WT/KO* samples, we observed a substantial shift of RPE65 from lower to higher molecular weight fractions in the *WT/KI* and *KI/KI* samples (Fig. 5 *A*, *Lower*), suggesting the formation of RPE65 protein aggregates. As shown in the final 13th fraction, less than 2% of the total RPE65 signal was present in the *WT/WT* and *WT/KO*, as opposed to the ∼15% in the *WT/KI* and ∼35% in the *KI/KI* mice (red arrows in Fig. 5 *A*, *Lower*). Our data suggest that the presence of the *D477G* mutant enhanced RPE65 protein-containing aggresomes.

D477G Mutation Affects the Subcellular Localization of RPE65. In the cell, RPE65 dimerizes and associates with the smooth endoplasmic reticulum (28–31). We investigated whether the subcellular localization of RPE65 was changed by the presence of a copy of the *D477G* mutation. Eye-cup homogenates from mice of indicated genotypes were fractionated into the cytosolic, membrane, nuclear, and insoluble fractions and immunoblotted

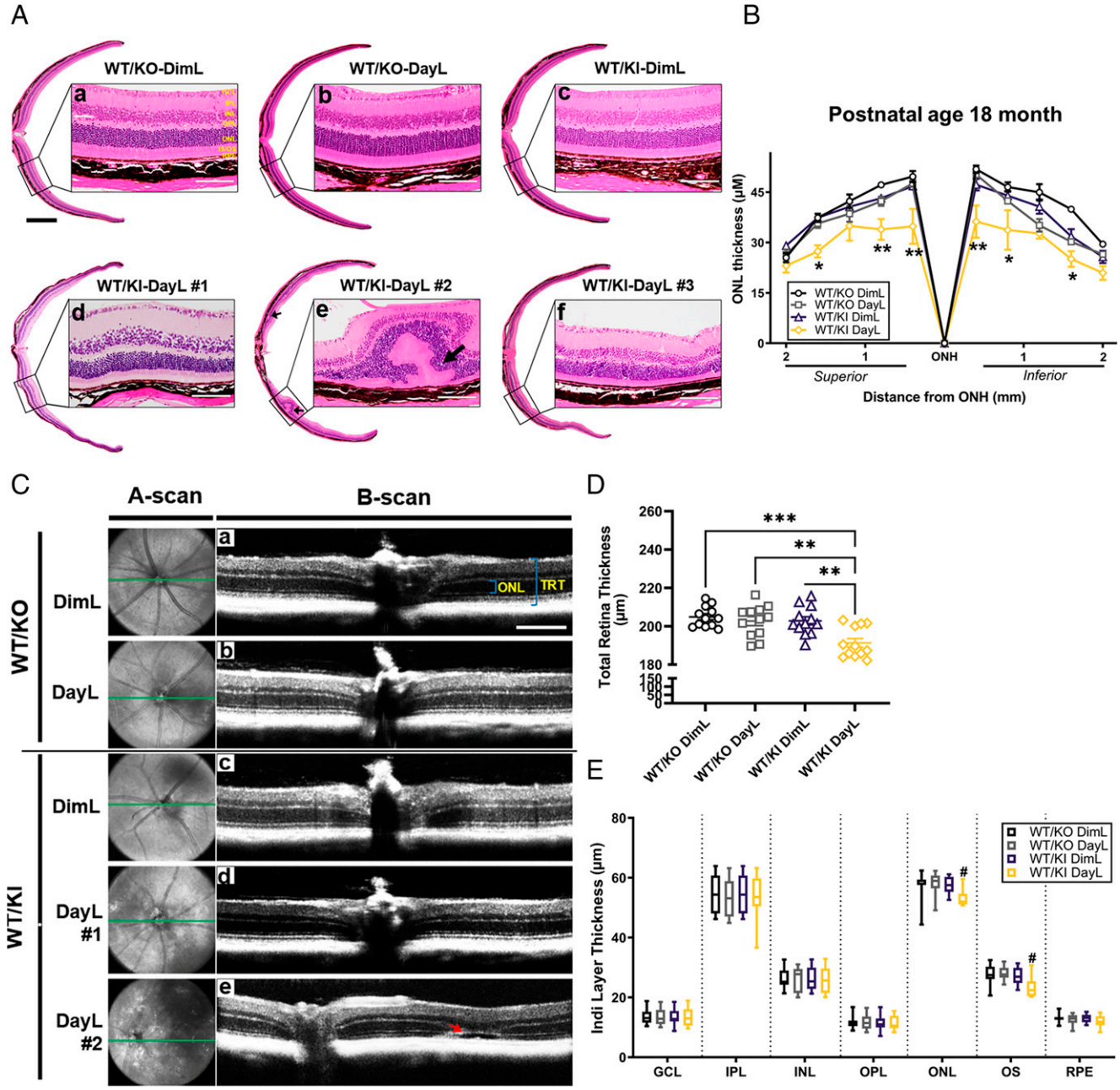

Fig. 3. Retina morphology in 18-mo-old DayL-exposed heterozygous *RPE65 D477G KI (WT/KI)* mice. (*A*) Representative images of hematoxylin, eosin, and saffron (H&E)-stained paraffin-embedded eye sections from mice of indicated genotypes. The lower panels (*d*–*f*) are retinal sections from three individual DayL-exposed *WT/KI* mice. Black arrows denote the development ORT in some of the *WT/KI*-DayL mice. (Scale bars, 400 μm for black, 100 μm for white.) (*B*) Histological measurement of ONL thickness in mice of indicated genotypes were taken from the optic nerve head (ONH) toward the periphery. Data depicted in spider graph shows a significant difference in ONL thickness only in the DayL-exposed *WT/KI* retinas, relative to the controls. (Scale bar, 100 μm.) (*C*) Representative SD-OCT images in live mice eyes of indicated genotypes show reduced TRT in the DayL-exposed *WT/KI* mice (*C*, *d* and *e*). A-scan shows the *en face* projection of the acquired retinal OCT volume (14 mm) centered on the optic nerve and illustrating the major blood vessels. B-scans are axial images showing various retinal layers made at the green line marked on the A-scans (*C*). Red arrow denotes the presence of ORT (*C*, *e*). (*D*) Quantification of TRT. (*E*) Quantification of individual layer thickness. Data are presented as mean ± SEM. Statistical analysis were performed with one-way ANOVA with Tukey's post hoc correction. Statistical significance is indicated by $^{**}P < 0.01$, $^{***}P < 0.001$, $^{\#}P < 0.0001$. *WT/KO* DimL, *WT/KO* DayL, and *WT/KI* DimL $n = 8$; *WT/KI* DayL $n = 6$. GCL, ganglion cell layer; INL, inner nuclear layer; IPL, inner plexiform layer.

for RPE65. As shown in Fig. 5*B*, most RPE65 was found in the cytosolic and membrane fractions. We validated the purity of each fraction by assessing the enrichment of cognate marker proteins: fibrillarin for nuclear and calnexin for endoplasmic reticulum fractions. A cytosolic abundance of RPE65 in the eye-cups of the *D477G WT/KI* and *KI/KI* mice was decreased relative to the *WT/WT* and *WT/KO* mice (Fig. 5*C*).

The subcellular distribution of RPE65 was examined by immunofluorescence in RPE flat mounts of age-matched animals. Immunolabeling of ZO-1 showed no disruptions in the RPE cell–cell junctions in any of the mouse groups (Fig. 5 *D*, *b*, *f*, *j*, and *n*). A difference was found in the expression levels and subcellular localization patterns of RPE65 in the *WT/KI* and *KI/KI* compared with the *WT/WT* and *WT/KO* mice. Under the same excitation intensity, the *WT/WT* eye-cup showed the highest RPE65 fluorescence (Fig. 5*E*). The signal distribution of RPE65 in the *WT/WT* RPE was mostly confluent and diffused equally (Fig. 5 *D*, *a*–*d*). The RPE65

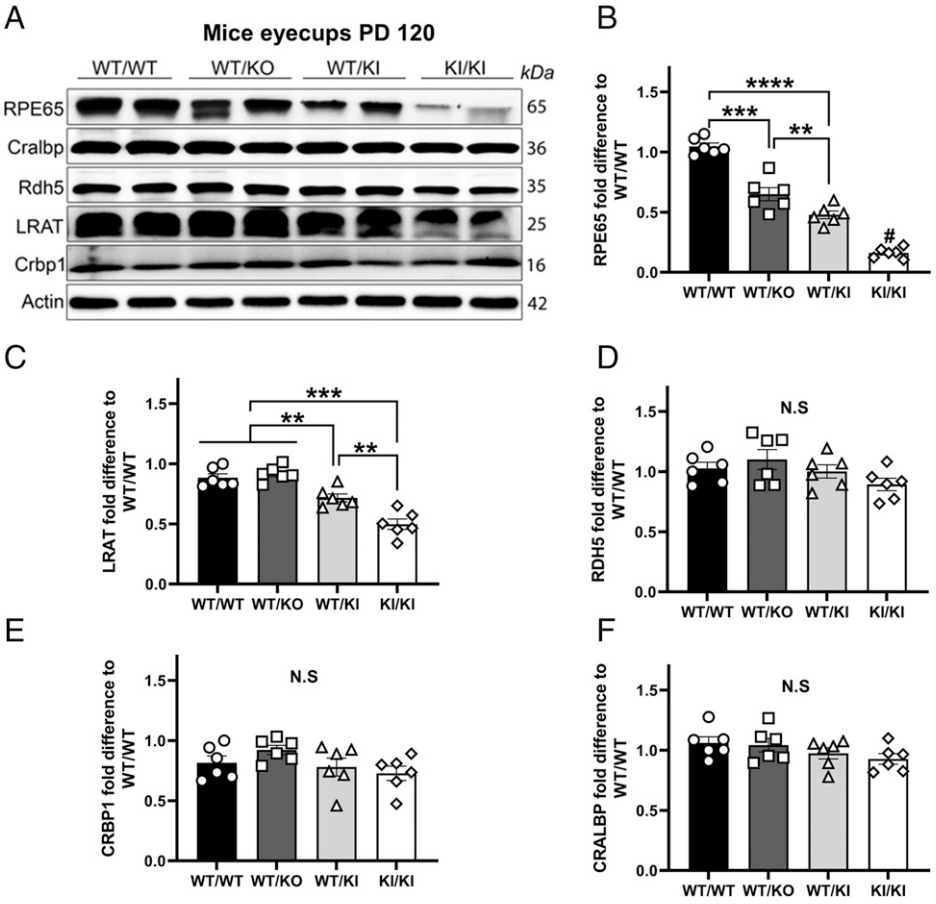

Fig. 4. *WT/KI* mice eye-cups exhibited relative lower protein expression of RPE65 and LRAT compared with *WT/KO* mice. (*A*) Representative Western blots for levels of RPE65 and other visual cycle related proteins in mice eye-cups at PD 120. (*B*) RPE65 levels in the *WT/KI*, *WT/KO*, and *KI/KI* at PD 120 presented as fold-change to *WT/WT* RPE65. (*C*) Fold-change of LRAT levels relative to *WT/WT*. (*D*–*F*) Fold-change of other visual cycle protein levels. Each lane contains pooled samples from six eye-cups from three individual mice. $n = 3$. Data are presented as mean ± SEM, $^{*}P < 0.05$, $^{**}P < 0.01$, $^{***}P < 0.001$, **** or $^{\#}P < 0.0001$ in one-way ANOVA with Tukey's post hoc comparison.

distribution pattern in the *WT/KO* was more concentrated around the cell center than the periphery and showed lower total cellular RPE65 intensity (Fig. 5 *D*, *e*–*h*). On the other hand, the RPE65 signal in the *WT/KI* eye-cups showed a different distribution. There was a notable reduction of RPE65 immuno-signals in the *WT/KI* RPE cells (Fig. 5*E*). The remaining RPE65 signal in the *WT/KI* RPE formed scalloped patches with areas of small uneven molted deposits collected at the cell periphery (Fig. 5 *D*, *i*), and the RPE65 signal was the lowest in the *KI/KI* eye-cups (Fig. 5 *D*, *m*). Our results suggest that the D477G mutation could affect RPE65 association with the ER membranes and mislocalization.

D477G Mutant Directly Interacts with WT RPE65. Plasmids expressing 6×His-tagged WT-RPE65 and FLAG-tagged D477G mutant were cotransfected into 293A-LRAT cells at 1:1 ratio, and coimmunoprecipitation (co-IP) was performed using the anti-His and anti-FLAG tag antibodies. As shown in Fig. 6*A*, WT-RPE65 was coprecipitated with FLAG-tagged D477G mutant in the cells expressing both the mutant and WT proteins. Reciprocal pull-down of the FLAG-tagged D477G mutant also coprecipitated His-tagged WT-RPE65, indicating a direct interaction of mutant D477G and WT-RPE65 proteins. Taken together, our results strongly suggest that the D477G mutant directly interacted with WT-RPE65, which may lead to aggregation, and mislocalization of WT-RPE65, in addition to the D477G mutant itself.

Association of D477G with WT-RPE65 Decreased the Stability of RPE65 Protein. To further investigate the consequence of D477G mutant protein interaction with WT-RPE65 protein, total RPE65 stability was examined in the presence and absence of the D477G mutant. The 293-LRAT cells were transfected with an equal copy number of the WT-RPE65, D477G transgenes using pVitro-2 bicistronic mammalian expression vector to ensure the equal ratio of transfected genes. At 18 h posttransfection, protein translation was interrupted by cycloheximide (CHX), and RPE65 levels were measured by Western blot analysis at 0, 6, and 12 h after the addition of CHX (Fig. 6 *B* and *C*). RPE65 protein levels declined rapidly in cells expressing D477G/D477G or WT/D477G, relative to those expressing WT/WT-RPE65 (Fig. 6*C*). The calculated half-life of WT/WT-RPE65 is ∼51 ± 5 h. In contrast, the WT/D477G and D477G/D477G showed a decreased half-life of 17 ± 2 h and 10 ± 3 h, respectively.

Previously published results by Choi's group (16) have observed that the D477G mutation facilitated mono- and di-ubiquitination of RPE65 and speculated that like other missense RPE65 mutants, the D477G variant also targets RPE65 for 26S proteasomal degradation (32). Cells were transfected with the vectors and treated with CHX and MG132, an inhibitor of the 26S proteasome, to investigate the proposed mechanism. As shown in Fig. 6*D*, MG132 treatment attenuated WT-RPE65 decrease to almost 100% of the initial expression level (Fig. 6*E*), while RPE65 degradation in WT/

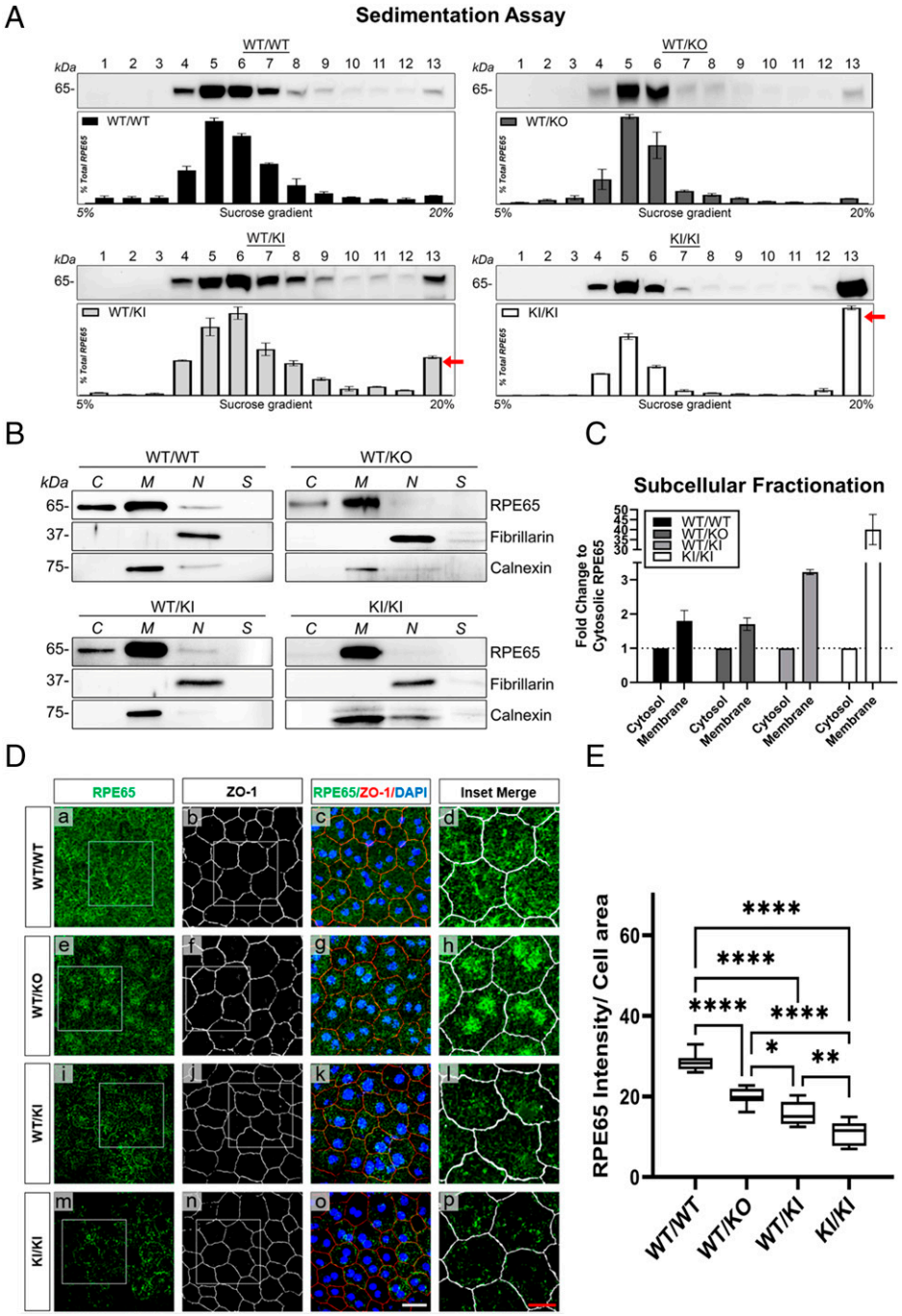

Fig. 5. D477G variant induces protein aggregation, and increases membrane association and mis-localization of RPE65 in vivo. Sucrose density sedimentation showed the formation of heavier protein aggregates in eye-cup homogenates from mice with indicated genotypes at 4 mo of age. (*A*) Representative blots with quantification bar graphs in the lower panels. RPE65 signal in each fraction was presented and plotted as percent of total RPE65 intensity. Fraction 1 is of the lowest density, and fraction 13 being the highest and the pellet. Red arrows indicate increased RPE65 signal in the 13th fraction in the *WT/KI* and *KI/KI* samples. $n = 3$. (*B* and *C*) Subcellular fractionation of RPE65 in *D477G* KI mice eye-cups. Fraction purity was analyzed using antibodies against indicated marker proteins. Fibrillarin: nuclear; calnexin: membrane. Representative Western blots (*B*) and quantification of RPE65 band intensity (*C*) in the membrane and cytosolic fraction. C, cytosolic; M, membrane; N, nuclear; S, cyto-skeleton. $n = 3$. (*D*) Immunofluorescence analyses of RPE65 in eye-cup flat-mounts. Green florescent RPE65 signal (*a*, *e*, *i*, and *m*) in mice of indicated genotypes. Zo-1 labels RPE cell boundary (*b*, *f*, *j*, and *n*) and DAPI (blue, *c*, *g*, *k*, and *o*) labels cell nuclei. (Scale bars, 30 μm for white and 10 μm for red.) (*E*) Quantification of average intracellular RPE65 signal. Data were presented as mean ± SEM, $*P < 0.05$, $**P < 0.01$, or $****P < 0.0001$ in one-way ANOVA with Tukey's post hoc comparison. $n = 6$ for each mice group.

D477G was only partially attenuated. In cells expressing D477G/D477G, the degree of RPE65 degradation was prevented by MG132 to a higher extent than that of the WT/D477G. Our results suggest that aside from the ubiquitin proteasomal pathway, the D477G-mediated RPE65 protein degradation involves other intracellular routes of protein clearance (Fig. 7).

Discussion

Although five independent KI mouse models have been generated for the *D477G* mutation, none of them recapitulated the retinal pathologies and degeneration exhibited by the affected patients (5, 15–17). In this study, we manipulated the environmental luminance to expose the retinal pathogenic effect of *D477G*. By

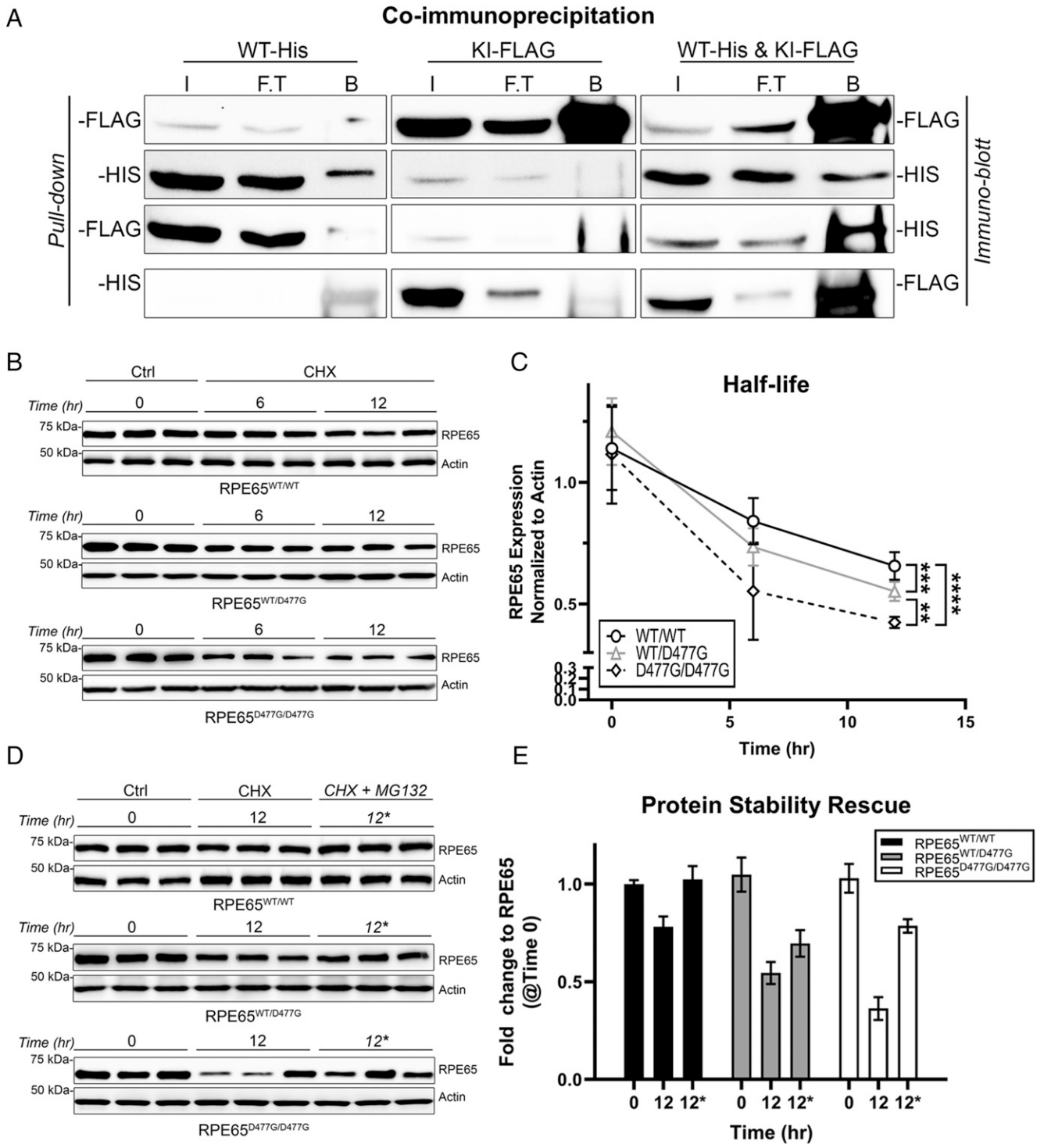

Fig. 6. D477G mutant associated with WT-RPE65 protein and predispose RPE65 to accelerated degradation. (*A*) Co-IP of His-tagged WT-RPE65 and FLAG-tagged D477G-variant showed the mutant to interact with the WT-RPE65. HEK293 cells were either singly or doubly transfected with constructs encoding FLAG-tagged D477G mutant and His-tagged WT-RPE65 protein. Reciprocal co-IP using either the anti-His or anti-FLAG antibody was performed in the above-mentioned transfected cell homogenates. Immunoblotting with either the anti-His or anti-FLAG antibody was used to determine coprecipitation. $n = 3$. I represents input (total protein extract); F.T. represents flow-through (the leftover unbound to beads antibody–protein fraction); and B represents bound (proteins that are bound by the antibodies and precipitated by the beads). (*B*) Western blot analysis of RPE65/D477G mutant protein in CHX-treated HEK293 cells. (*C*) Diagram depicting mean RPE65 degradation curves over 0, 6, and 12 h after the addition of CHX. $n = 3$. (*D*) Western blot analysis of RPE65 showing partial degradation arrested in cells coexpressing D477G mutant and WT-RPE65 by treatment with MG132 in the presence of CHX at indicated times. (*E*) Quantitative evaluation of RPE65 protein levels in cells expressing the indicated constructs and respective treatments. $n = 3$. All data are presented as means ± SEM $^*P < 0.05$, $^{**}P < 0.01$, $^{***}P < 0.001$, or $^{****}P < 0.0001$ in one-way ANOVA with Tukey's post hoc comparison.

making direct comparisons of the phenotypic changes of the *D477G* KI heterozygotes (*WT/KI*) with heterozygous *RPE65* KO (*WT/KO*) mice, we provided functional, morphological, in vitro, and in vivo molecular evidences that support the dominant-negative nature of the D477G mutant. In each tested instance, we showed that the adverse cellular consequence of the D477G mutant coexpressed with WT-RPE65 far exceeded that of losing a single allele of WT-RPE65 and disapproved the retinal dysfunction hypothesis that retinal pathologies in heterozygous D477G patients may be caused by haploinsufficiency.

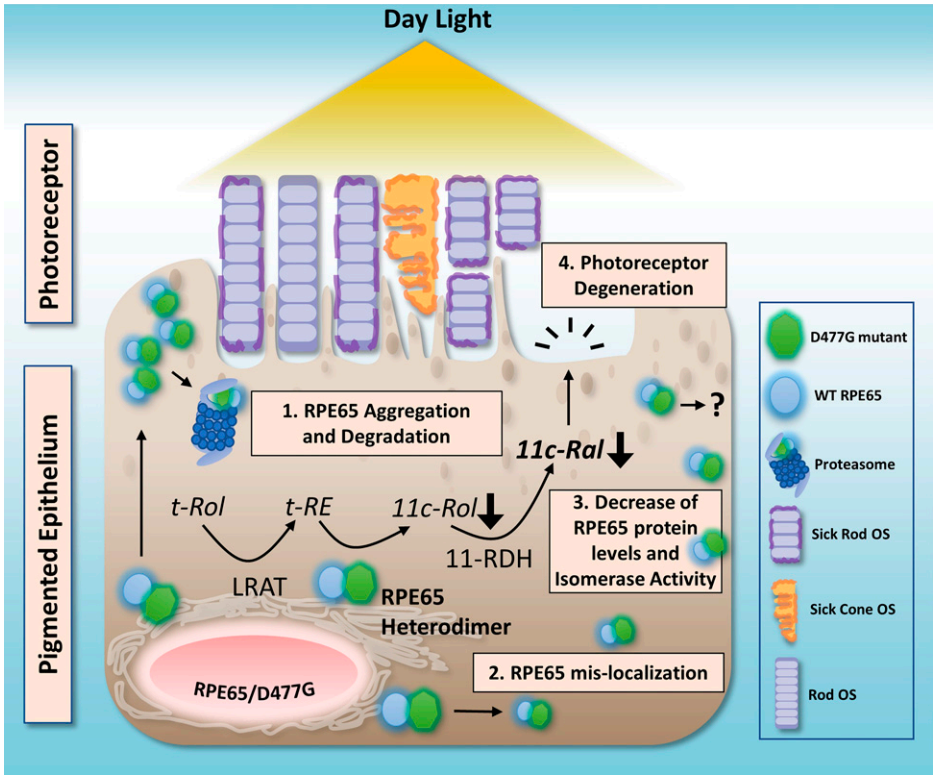

Fig. 7. Schematic diagram showing proposed pathogenesis of dominant acting *D477G RPE65* in the heterozygote KI mice exposed to DayL luminance. In the RPE of *WT/KI* mice, the *D477G* variant associates with WT-RPE65, resulting in RPE65 mislocalization and accelerated degradation of total RPE65. Moreover, abnormal protein aggregates are formed in the presence of the mutant. Under DayL luminance, the increase in demand for chromophore production in the RPE is unfulfilled by the D477G *WT/KI* RPE, which exhibited decreased RPE65 expression, leading to insufficient 11-*cis*-RAL regeneration. Both constitutive activation from the unligand opsin in the *WT/KI* retina and the toxic aggregation of RPE65 in *WT/KI* RPE together induce retina stress and accentuate the retina pathology. RPE65, retinal pigmented epithelium 65-kDa protein; *t-RE*, all-*trans*-retinyl-ester; *t-Rol*, all-*trans*-retinol; 11*c-Ral*, 11-*cis*-retinal; 11*c-Rol*, 11-*cis*-retinol; 11-RDH, 11-*cis*-retinol dehydrogenase; ?, additional mechanisms responsible for D477G mediated reduced isomerase activity.

Light is often manipulated in laboratory animals to drive ocular pathologies through increasing retinal oxidative stress (33, 34). In an adRP causing a rhodopsin P23H mutant mouse model, the retina degeneration progressed faster when the mice were raised under cyclical light, whereas the degeneration slowed in mice raised in the dark (35). Similarly, a direct light effect on the rate of PR loss was reported in the retinal degeneration slow, another inheritable retinopathy (IR) mouse model (36). More recently, Li et al. (17) employed a nonstandard housing luminance of 500 lx on their *D477G* KI mouse model to induce pathogenic phenotypes in the *WT/KI* mice. However, only minor ERG decline was noted in the homozygous KI (*KI/KI*) mice, which does not explain the phenotypes in D477G-affected patients. It has been well documented that repeated exposure to excessive environmental illumination causes chronic retinal degeneration in the otherwise healthy retina (37–39), exacerbates IR (40–42), and is one of the major risk factors for the development of age-related macular degeneration (39, 43). Conversely, protection from light is reported to slow the progress of retinal degeneration in many of the above-mentioned reports (40, 44).

Because light of excessive brightness can damage the normal retina (44), while insufficient light will not produce an aggravating effect as observed by Li et al. (17), we exposed our adult mice to 2,000 lx, a light intensity comparable to that of the indoor or a cloud covered day luminance experienced by humans (45, 46). In the RPE65-null mice, an opsin lacking 11-*cis*-RAL lead to constant low-level activation of phototransduction, consequently increased cellular stress, and accelerated retinal degeneration in a light intensity-dependent manner (47, 48). Likewise, we used light to hasten the visual cycle activity in the RPE through the acceleration of phototransduction and 11-*cis*-RAL expenditure at the PR. The increased demand for 11-*cis*-RAL by the PR, with the aforementioned light-induced oxidative stress, may be sufficient to incite the onset of D477G-mediated pathologies. To exclude the effect of phototoxicity on the retina, we pretested the 2,000-lx light on WT littermates up to 18 mo of age and detected no difference in retinal function and morphology in the mice exposed to 2,000 lx than those maintained under DimL (*SI Appendix*, Figs. S1–S3).

Indeed, *D477G* KI heterozygotes maintained under DayL manifested reduced retinal ERG amplitudes and architectural defects, such as OS, ONL thinning, and ORT, recapitulating anomalies detected in the D477G patients (Figs. 1–3) (5, 12, 13). Furthermore, when exposed to DayL intensity, the disease progression of the *WT/KI* mice recapitulated those in a majority of the D477G patients, with the disease onsets around mid-adulthood between the ages of 40 and 50 y, analogous to mice around 15 to 18 mo of age (49). There are the occasional late-onset D477G adRP patients (11). Our previous report showed a delayed a-wave recovery rate in the 9-mo-old *WT/KI* mice, consistent with other reports (11, 14, 16). In this study, we found that the delayed a-wave recovery persisted in the 12- and 18-mo-old *WT/KI* mice, which is the study's endpoint (Fig. 2 *A* and *B*). Compared with littermates raised under DimL, housing the *WT/KI* mice under DayL further slowed the recovery rate of rod photosensitivity (Fig. 2*B*). Our data suggested that the visual cycle in the *WT/KI* RPE was impaired prior to the onset of PR dysfunction. This retinal functional decline in the

WT/KI model is consistent with that of the D477G adRP patients, the initial onset of night blindness predating functional vision loss (14).

In the previous studies, the total RPE65 protein levels in the *D477G WT/KI* mouse models were reduced to ∼45 to 50% of that in the *WT/WT* mice (14, 16, 17). Comparing the levels of RPE65 in the *WT/KI*, *WT/KO*, and *KI/KI* mice to the *WT/WT* littermates, we also observed a similar fold reduction of RPE65 protein in the 4-mo-old *WT/KI* eye-cups (Fig. 4*B*). Our results suggested that the D477G variant adversely impacted WT-RPE65 protein levels as the *WT/KI* eye-cups showed significantly lower RPE65 levels than the *WT/WT* and *WT/KO* mice (Fig. 4*B*). In the same 4-mo-old mice, we saw a concomitant decline in the LRAT protein levels (Fig. 4*C*), suggesting that aside from lowering RPE65 protein levels as reported by others (5, 11), the D477G mutant might impact other components of the visual cycle.

Multiple groups speculated that the charged aspartic acid at position 477 acts as a "gatekeeper" residue for maintaining proper RPE65 protein interactions (14, 16, 17). We report that replacing the aspartic acid with glycine in RPE65 indeed induced protein aggregation, as evidenced by the sedimentation study (Fig. 5*A*). Both subcellular fractionation and immunofluorescence assays in the *WT/KI* eye-cups indicated that the mutant alters RPE65 subcellular distribution (Fig. 5 *B*–*D*). Moreover, co-IP demonstrated the direct association of the D477G protein and WT RPE65 protein (Fig. 6*A*). Our molecular approaches demonstrated protein–protein interactions of WT-RPE65 and D477G mutant, as previously predicted (5, 16). We showed that the direct interaction of D477G mutant with WT-RPE65 reduced cellular RPE65 stability (Fig. 6 *B* and *D*). In addition, as a membrane-bound isomerase, RPE65 mislocalization could impair its activity (50, 51). Indeed, we found the *WT/KI* RPE to exhibit lower 11-*cis*-ROL production activity than the *WT/KO* RPE (Fig. 2*D*), and identified increased free opsin in the daylight-exposed *WT/KI* retina (*SI Appendix*, Fig. S4).

WT-RPE65 and mutant protein complex aggregation have been reported in many other recessive RPE65 mutants, such as L22P, T101I, and L408P (32). However, unlike the previous studies on these mutants (16), treatment with the proteasome inhibitor MG132 did not fully rescue RPE65 protein levels in cells transfected with *D477G/WT* or *D477G/D477G* vectors (Fig. 6*C*), suggesting that the disposal of the D477G variant may not be solely mediated by proteasomal degradation alone. In addition, the degree of rescue after MG132 treatment in *WT/KI* was paradoxically lower than that of the *KI/KI* transfected cells. This suggests that different cellular pathways mediate the degradation of the D477G/WT RPE65 dimers. Further studies are necessary to elucidate alternative pathways, such as chaperone protein rehabilitation or autophagy at work to maintain RPE65 homeostasis.

Previous publications on RPE65 recessive missense mutants showed that 20 to 30% of WT-RPE65 provided an adequate level of chromophore required to sustain functional vision in mice (52, 53). When compared with the *WT/WT*, *D477G WT/KI* RPE expresses 35 to 45% (Fig. 4*B*), and *WT/KO* expresses about 55 to 60% of total RPE65 (54); the light-driven phenotype in the *WT/KI* but not in the *WT/KO* cannot be completely explained by decreased levels of RPE65 protein alone. Future studies are required to elucidate the other avenues where the D477G mutant impacts RPE65 isomerase activity. As suggested by numerous other studies, the abnormal protein aggregates formed in the *WT/KI* eye-cups could cause further cellular stress or cellular toxicity to the RPE cells (6, 13, 16). Interestingly, we observed an up-regulation of GFAP expression in the *WT/KI* mouse retina, exacerbated by 2,000-lx light exposure (*SI Appendix*, Fig. S5). This sign of increased retina stress in the D477G KI mouse opens up a new line of investigation in our future studies. Mutations in other visual cycle-related enzymes—such as Rdh10 (55), Rlbp1 (56), and Rgr (57), which are known to cause retinal degenerations in humans—are unable to be recapitulated in the mice models. However, just like the *D477G* KI, these models all display some degree of dark-adaptation delay. Therefore, we hypothesized that changing the light condition might also incite retinal degenerative features in these mice.

Intrafamilial clinical heterogeneity is a well-known yet unexplained phenomenon observed in patients of IR. The variable intensity of light luminance a person experiences may explain the variable age of onset and disease severity in the D477G patient population and perhaps in other forms of IR (58). Alternatively, but not mutually exclusive, the variable phenotypic presentation in our light-exposed mouse model and the reported variable genetic penetrance associated with the human c.1430A > G mutation strongly suggest that additional environmental factors may modulate disease presentation. Light exposure as a trigger for disease outcome can easily be targeted as a predisposing stressor for avoidance in multiple forms of IR.

In conclusion, we demonstrated that physiological relevant environmental light intensity (2,000 lx) induced the manifestation of retinal dysfunction and degeneration in the heterozygous (*WT/KI*) but not heterozygous RPE65 KO (*WT/KO*) mice. Our results implicate that ambient light could be a causative factor that enhances disease onset and progression in affected humans and rodents carrying a single copy of the D477G mutant. Our findings also revealed that D477G is a dominant-negative mutation, a possible mechanism by which a single copy of D477G causes retinal dystrophy. Moreover, our studies revealed a possible connection between environmental luminance on the progression of IR.

Materials and Methods

Animals. All animal experiments were approved by the Institutional Animal Care and Use Committee of the University of Oklahoma Health Sciences Center (Oklahoma City, OK), and performed following the guidelines of the Association for Research in Vision and Ophthalmology Statement for the Use of Animals in Ophthalmic and Vision Research. The *RPE65 D477G* KI mouse model was generated by our group previously (15). *RPE65* KO mice were a kind gift from Michael Redmond, National Eye Institute, Bethesda, MD (10). Heterozygous KO mice were obtained by crossing homozygous *RPE65* KO mice with WT C57BL/6J. All mice were in the C57BL/6J background and were maintained in standard housing conditions with 12-h light/dark cycles and food and water ad libitum. The *rd8* mutation in the *Crb1* gene was excluded from all F1 generations by Sanger sequencing (59).

Physiological Relevant DayL Treatment. For chronic light exposure at physiological relevant luminance of 2,000 lx, the experimental mice were first raised at regular vivarium light to around 3 mo of age. Then, the *D477G* KI heterozygotes (*WT/KI*) and the *RPE65* KO heterozygotes (*WT/KO*) were grouped randomly to be maintained in 12-h DayL (∼2,000 lx)/12-h dark or in 12-h regular vivarium DimL (∼100 lx)/12-h dark conditions (*SI Appendix*, Fig. S1). For details of the 2,000-lx light cubicle set up, see *SI Appendix*.

Electroretinography. Full-field ERG was conducted with *D477G* KI and *RPE65* KO heterozygote mice, maintained under either DimL or DayL, at the ages of 3, 6, 9, 12, 15, and 18 mo. All ERGs were recorded with the Espion E3 system Ganzfeld Color Dome system (Diagnosys); for details, see *SI Appendix*.

SD-OCT. Mice were anesthetized and their pupils were dilated. Artificial tears (Systane Ultra, Alcon) were used to maintain corneal hydration and clarity. The retinal thickness was measured using a SD-OCT device (Bioptigen) following a previously established method (60). For details, see *SI Appendix*.

RPE65 Isomerase Activity Assay. The isomerase activity of RPE65 was measured using HPLC, as described previously (61). For details, see *SI Appendix*.

HPLC Measurement of Endogenous Retinoids. Endogenous 11-*cis*-RAL in mice eye-cups was analyzed using HPLC, as described previously (62). For details, see *SI Appendix*.

Immunoblotting. Western blot analysis was performed as described previously (63); for details, see *SI Appendix*. The antibodies used are listed in *SI Appendix*.

Sucrose Velocity Sedimentation. Nonreducing velocity sedimentation was performed following a documented method (64), with modifications on extracts from the eye-cups of mice. For details, see *SI Appendix*.

Subcellular Fractionation. All details regarding the assay and analyses are in *SI Appendix*.

Construction of Pvitro-2 Heterozygous RPE65-WT/D477G. Details on vector construction are in *SI Appendix*.

Immunoprecipitation. Reciprocal co-IP was performed with anti-His and anti-FLAG antibodies. Plasmids expressing His-tagged WT-RPE65 and FLAG-tagged D477G mutant-RPE65 were either individually or cotransfected at an equal molar ratio into 293A-LRAT cells, a cell line stably expressing human LRAT (9), using polyethyleneimine (PEI; Polysciences) at 1 mg/mL, pH 7.4, 2:1 PEI/DNA ratio (61). AT 48 h posttransfection, total cellular proteins were extracted. Co-IP was performed following manufacturer's protocol (Santa Cruz); for details see *SI Appendix*.

Protein Stability Assay. The assay was performed following a previously published method (65); for details see *SI Appendix*.

Histology. All details regarding the assay and analyses are in *SI Appendix*.

Immunostaining and Confocal Imaging. All details regarding the immunofluorescence assays, image acquisition, and analyses are in *SI Appendix*.

Statistical Analysis. GraphPad Prism 7.0 software (GraphPad Software) was used for all statistical analyses and graphical depiction of the data. Results are expressed as mean ± SEM. A two-tailed unpaired Student's *t* test was used for two-group comparisons. In experiments with more than two experimental groups, a one-way ANOVA with Tukey's post hoc comparison was used unless stated otherwise. *P* values of less than or equal to 0.05 were considered statistically significant.

Data Availability. All study data are included in the main text and *SI Appendix*.

ACKNOWLEDGMENTS. We thank Dr. Robert D. Foremen (University of Oklahoma College of Medicine) and John Wood for their technical editing and manuscript revision; Dr. Shannon Conley and Dr. Rui Cheng for the generous sharing of their practical expertise; and the animal teams at the University of Oklahoma Health Sciences Center for their dedication to our animal welfare. We also thank the technical support from the Diabetic Animal Core, Histology and Image Core, supported by Centers of Biomedical Research Excellence Grant GM122744, and the Vision Core supported by NEI Grant P30 (EY021725). This study was supported by NIH Grants EY018659, EY019309, EY012231, EY028949, EY032930, and EY032931.

1. F. P. M. Cremers, C. J. F. Boon, K. Bujakowska, C. Zeitz, Special issue introduction: Inherited retinal disease: Novel candidate genes, genotype-phenotype correlations, and inheritance models. *Genes (Basel)* **9**, 215 (2018).
2. M. Hanany, C. Rivolta, D. Sharon, Worldwide carrier frequency and genetic prevalence of autosomal recessive inherited retinal diseases. *Proc. Natl. Acad. Sci. U.S.A.* **117**, 2710–2716 (2020).
3. H. Morimura *et al.*, Mutations in the RPE65 gene in patients with autosomal recessive retinitis pigmentosa or Leber congenital amaurosis. *Proc. Natl. Acad. Sci. U.S.A.* **95**, 3088–3093 (1998).
4. M. Aoun *et al.*, Inherited retinal diseases due to *RPE65* variants: From genetic diagnostic management to therapy. *Int. J. Mol. Sci.* **22**, 7207 (2021).
5. S. J. Bowne *et al.*, A dominant mutation in RPE65 identified by whole-exome sequencing causes retinitis pigmentosa with choroidal involvement. *Eur. J. Hum. Genet.* **19**, 1074–1081 (2011).
6. D. A. Thompson *et al.*, Genetics and phenotypes of RPE65 mutations in inherited retinal degeneration. *Invest. Ophthalmol. Vis. Sci.* **41**, 4293–4299 (2000).
7. X. Cai, S. M. Conley, M. I. Naash, RPE65: Role in the visual cycle, human retinal disease, and gene therapy. *Ophthalmic Genet.* **30**, 57–62 (2009).
8. G. Moiseyev, Y. Chen, Y. Takahashi, B. X. Wu, J. X. Ma, RPE65 is the isomerohydrolase in the retinoid visual cycle. *Proc. Natl. Acad. Sci. U.S.A.* **102**, 12413–12418 (2005).
9. Y. Takahashi, G. Moiseyev, Y. Chen, J. X. Ma, Identification of conserved histidines and glutamic acid as key residues for isomerohydrolase activity of RPE65, an enzyme of the visual cycle in the retinal pigment epithelium. *FEBS Lett.* **579**, 5414–5418 (2005).
10. T. M. Redmond *et al.*, Rpe65 is necessary for production of 11-*cis*-vitamin A in the retinal visual cycle. *Nat. Genet.* **20**, 344–351 (1998).
11. P. F. Kenna *et al.*, Advanced late-onset retinitis pigmentosa with dominant-acting D477G RPE65 mutation is responsive to oral synthetic retinoid therapy. *BMJ Open Ophthalmol.* **5**, e000462 (2020).
12. S. Hull, R. Mukherjee, G. E. Holder, A. T. Moore, A. R. Webster, The clinical features of retinal disease due to a dominant mutation in RPE65. *Mol. Vis.* **22**, 626–635 (2016).
13. R. Jauregui, K. S. Park, S. H. Tsang, Two-year progression analysis of RPE65 autosomal dominant retinitis pigmentosa. *Ophthalmic Genet.* **39**, 544–549 (2018).
14. A. S. Kiang *et al.*, Properties and therapeutic implications of an enigmatic D477G RPE65 variant associated with autosomal dominant retinitis pigmentosa. *Genes (Basel)* **11**, 1420 (2020).
15. Y. Shin, G. Moiseyev, D. Chakraborty, J.-X. Ma, A dominant mutation in Rpe65, D477G, delays dark adaptation and disturbs the visual cycle in the mutant knock-in mice. *Am. J. Pathol.* **187**, 517–527 (2017).
16. E. H. Choi *et al.*, Insights into the pathogenesis of dominant retinitis pigmentosa associated with a D477G mutation in RPE65. *Hum. Mol. Genet.* **27**, 2225–2243 (2018).
17. Y. Li *et al.*, Aberrant RNA splicing is the major pathogenic effect in a knock-in mouse model of the dominantly inherited c.1430A>G human RPE65 mutation. *Hum. Mutat.* **40**, 426–443 (2019).
18. W. Sharif, Z. Sharif, Leber's congenital amaurosis and the role of gene therapy in congenital retinal disorders. *Int. J. Ophthalmol.* **10**, 480–484 (2017).
19. X. Wang, C. Yu, R. T. Tzekov, Y. Zhu, W. Li, The effect of human gene therapy for RPE65-associated Leber's congenital amaurosis on visual function: A systematic review and meta-analysis. *Orphanet J. Rare Dis.* **15**, 49 (2020).
20. S. G. Jacobson *et al.*, Improvement and decline in vision with gene therapy in childhood blindness. *N. Engl. J. Med.* **372**, 1920–1926 (2015).
21. A. V. Cideciyan *et al.*, Human retinal gene therapy for Leber congenital amaurosis shows advancing retinal degeneration despite enduring visual improvement. *Proc. Natl. Acad. Sci. U.S.A.* **110**, E517–E525 (2013).
22. F. Marlhens *et al.*, Mutations in RPE65 cause Leber's congenital amaurosis. *Nat. Genet.* **17**, 139–141 (1997).
23. J. A. Galvin, G. A. Fishman, E. M. Stone, R. K. Koenekoop, Evaluation of genotype-phenotype associations in Leber congenital amaurosis. *Retina* **25**, 919–929 (2005).
24. J. Hoh Kam, A. Lynch, R. Begum, A. Cunea, G. Jeffery, Topical cyclodextrin reduces amyloid beta and inflammation improving retinal function in ageing mice. *Exp. Eye Res.* **135**, 59–66 (2015).
25. S. Ma *et al.*, Loss of mTOR signaling affects cone function, cone structure and expression of cone specific proteins without affecting cone survival. *Exp. Eye Res.* **135**, 1–13 (2015).
26. A. V. Kolesnikov, J. Fan, R. K. Crouch, V. J. Kefalov, Age-related deterioration of rod vision in mice. *J. Neurosci.* **30**, 11222–11231 (2010).
27. J. Gresh, P. W. Goletz, R. K. Crouch, B. Rohrer, Structure-function analysis of rods and cones in juvenile, adult, and aged C57bl/6 and Balb/c mice. *Vis. Neurosci.* **20**, 211–220 (2003).
28. P. D. Kiser, M. Golczak, D. T. Lodowski, M. R. Chance, K. Palczewski, Crystal structure of native RPE65, the retinoid isomerase of the visual cycle. *Proc. Natl. Acad. Sci. U.S.A.* **106**, 17325–17330 (2009).
29. P. D. Kiser, K. Palczewski, Membrane-binding and enzymatic properties of RPE65. *Prog. Retin. Eye Res.* **29**, 428–442 (2010).
30. Y. Takahashi *et al.*, Identification of a novel palmitylation site essential for membrane association and isomerohydrolase activity of RPE65. *J. Biol. Chem.* **284**, 3211–3218 (2009).
31. E. Trudel, S. Beaufils, A. Renault, R. Breton, C. Salesse, Binding of RPE65 fragments to lipid monolayers and identification of its partners by glutathione S-transferase pull-down assays. *Biochemistry* **45**, 3337–3347 (2006).
32. S. Li *et al.*, Rescue of enzymatic function for disease-associated RPE65 proteins containing various missense mutations in non-active sites. *J. Biol. Chem.* **289**, 18943–18956 (2014).
33. Y. Ozawa, Oxidative stress in the light-exposed retina and its implication in age-related macular degeneration. *Redox Biol.* **37**, 101779 (2020).
34. M. Kamoshita *et al.*, Lutein acts via multiple antioxidant pathways in the photo-stressed retina. *Sci. Rep.* **6**, 30226 (2016).
35. M. Wang, T. T. Lam, M. O. Tso, M. I. Naash, Expression of a mutant opsin gene increases the susceptibility of the retina to light damage. *Vis. Neurosci.* **14**, 55–62 (1997).
36. S. Sanyal, R. K. Hawkins, Development and degeneration of retina in rds mutant mice: Effects of light on the rate of degeneration in albino and pigmented homozygous and heterozygous mutant and normal mice. *Vision Res.* **26**, 1177–1185 (1986).
37. D. T. Organisciak, D. K. Vaughan, Retinal light damage: Mechanisms and protection. *Prog. Retin. Eye Res.* **29**, 113–134 (2010).
38. M. Kaitz, E. Auerbach, Retinal degeneration in RCS rats raised under ambient light levels. *Vision Res.* **19**, 79–81 (1979).
39. M. A. Contín, M. M. Benedetto, M. L. Quinteros-Quintana, M. E. Guido, Light pollution: The possible consequences of excessive illumination on retina. *Eye (Lond.)* **30**, 255–263 (2016).
40. D. M. Paskowitz, M. M. LaVail, J. L. Duncan, Light and inherited retinal degeneration. *Br. J. Ophthalmol.* **90**, 1060–1066 (2006).
41. K. Rascher *et al.*, Light deprivation slows but does not prevent the loss of photoreceptors in taurine transporter knockout mice. *Vision Res.* **44**, 2091–2100 (2004).

42. J. Chen, M. I. Simon, M. T. Matthes, D. Yasumura, M. M. LaVail, Increased susceptibility to light damage in an arrestin knockout mouse model of Oguchi disease (stationary night blindness). *Invest. Ophthalmol. Vis. Sci.* **40**, 2978–2982 (1999).
43. K. J. Cruickshanks, R. Klein, B. E. K. Klein, D. M. Nondahl, Sunlight and the 5-year incidence of early age-related maculopathy: The beaver dam eye study. *Arch. Ophthalmol.* **119**, 246–250 (2001).
44. M. M. LaVail, G. M. Gorrin, M. A. Repaci, L. A. Thomas, H. M. Ginsberg, Genetic regulation of light damage to photoreceptors. *Invest. Ophthalmol. Vis. Sci.* **28**, 1043–1048 (1987).
45. A. Stockman, L. T. Sharpe, Into the twilight zone: The complexities of mesopic vision and luminous efficiency. *Ophthal. Physiol. Opt.* **26**, 225–239 (2006).
46. W. T. Keenan *et al.*, A visual circuit uses complementary mechanisms to support transient and sustained pupil constriction. *eLife* **5**, e15392 (2016).
47. J. Fan, M. L. Woodruff, M. C. Cilluffo, R. K. Crouch, G. L. Fain, Opsin activation of transduction in the rods of dark-reared Rpe65 knockout mice. *J. Physiol.* **568**, 83–95 (2005).
48. M. L. Woodruff *et al.*, Spontaneous activity of opsin apoprotein is a cause of Leber congenital amaurosis. *Nat. Genet.* **35**, 158–164 (2003).
49. P. Sengupta, The laboratory rat: Relating Its age with human's. *Int. J. Prev. Med.* **4**, 624–630 (2013).
50. C. P. Hamel *et al.*, A developmentally regulated microsomal protein specific for the pigment epithelium of the vertebrate retina. *J. Neurosci. Res.* **34**, 414–425 (1993).
51. H. Sagara, K. Hirosawa, Monoclonal antibodies which recognize endoplasmic reticulum in the retinal pigment epithelium. *Exp. Eye Res.* **53**, 765–771 (1991).
52. M. Samardzija *et al.*, R91W mutation in Rpe65 leads to milder early-onset retinal dystrophy due to the generation of low levels of 11-*cis*-retinal. *Hum. Mol. Genet.* **17**, 281–292 (2008).
53. Y. Li *et al.*, Mouse model of human RPE65 P25L hypomorph resembles wild type under normal light rearing but is fully resistant to acute light damage. *Hum. Mol. Genet.* **24**, 4417–4428 (2015).
54. A. L. Lyubarsky *et al.*, Mole quantity of RPE65 and its productivity in the generation of 11-*cis*-retinal from retinyl esters in the living mouse eye. *Biochemistry* **44**, 9880–9888 (2005).
55. B. Sahu *et al.*, Conditional ablation of retinol dehydrogenase 10 in the retinal pigmented epithelium causes delayed dark adaption in mice. *J. Biol. Chem.* **290**, 27239–27247 (2015).
56. J. R. Lima de Carvalho Jr. *et al.*, Effects of deficiency in the *RLBP1*-encoded visual cycle protein CRALBP on visual dysfunction in humans and mice. *J. Biol. Chem.* **295**, 6767–6780 (2020).
57. T. Maeda *et al.*, Evaluation of the role of the retinal G protein-coupled receptor (RGR) in the vertebrate retina in vivo. *J. Neurochem.* **85**, 944–956 (2003).
58. F. Simonelli *et al.*, Intrafamilial clinical heterogeneity associated with a novel mutation of the retinal degeneration slow/peripherin gene. *Ophthalmic Res.* **39**, 255–259 (2007).
59. M. J. Mattapallil *et al.*, The Rd8 mutation of the Crb1 gene is present in vendor lines of C57BL/6N mice and embryonic stem cells, and confounds ocular induced mutant phenotypes. *Invest. Ophthalmol. Vis. Sci.* **53**, 2921–2927 (2012).
60. F. Qiu *et al.*, Pathogenic role of human C-reactive protein in diabetic retinopathy. *Clin. Sci. (Lond.)* **134**, 1613–1629 (2020).
61. Y. Takahashi, G. Moiseyev, J. X. Ma, Identification of key residues determining isomerohydrolase activity of human RPE65. *J. Biol. Chem.* **289**, 26743–26751 (2014).
62. V. V. Malechka, G. Moiseyev, Y. Takahashi, Y. Shin, J. X. Ma, Impaired rhodopsin generation in the rat model of diabetic retinopathy. *Am. J. Pathol.* **187**, 2222–2231 (2017).
63. F. Qiu *et al.*, Fenofibrate-loaded biodegradable nanoparticles for the treatment of experimental diabetic retinopathy and neovascular age-related macular degeneration. *Mol. Pharm.* **16**, 1958–1970 (2019).
64. R. Zulliger, S. M. Conley, M. L. Mwoyosvi, M. R. Al-Ubaidi, M. I. Naash, Oligomerization of Prph2 and Rom1 is essential for photoreceptor outer segment formation. *Hum. Mol. Genet.* **27**, 3507–3518 (2018).
65. Y. Takahashi, Y. Chen, G. Moiseyev, J. X. Ma, Two point mutations of RPE65 from patients with retinal dystrophies decrease the stability of RPE65 protein and abolish its isomerohydrolase activity. *J. Biol. Chem.* **281**, 21820–21826 (2006).